Adsorption and Desorption of HCl on Pt(111)

John L. Daschbach,[†] Jooho Kim,[‡] Patrick Ayotte,[§] R. Scott Smith,[‡] and Bruce D. Kay*[,‡]

Environmental Molecular Sciences Laboratory and Fundamental Science Division, Pacific Northwest National Laboratory, P.O. Box 999, Mail Stop K8-88, Richland, Washington 99352, and Département de Chimie, Université de Sherbrooke, 2500 Boul. Université, Sherbrooke, Québec J1K 2R1, Canada

Received: April 26, 2005; In Final Form: June 14, 2005

The adsorption and desorption of HCl on Pt(111) is investigated by temperature programmed desorption, infrared reflection absorption spectroscopy, and low energy electron diffraction. Five peaks are identified in the desorption spectra prior to the onset of multilayer desorption. At low coverage ($\Theta < 0.25$ monolayers (ML)), desorption peaks at ~135 and 200 K are observed and assigned to recombinative desorption of dissociated HCl. At higher coverages, desorption peaks at 70, 77, and 84 K are observed. These peaks are assigned to the desorption of molecularly adsorbed HCl. The infrared spectra are in agreement with these assignments and show that HCl deposited at 20 K is amorphous but crystallizes when heated above 60 K. Kinetic analysis of the desorption spectra reveals a strong repulsive coverage dependence for the desorption energy of the low coverage features ($\Theta < 0.25$ ML). The diffraction data indicate that at low temperature the adsorbed HCl clusters into ordered islands with a (3×3) structure and a local coverage of 4/9 with respect to the Pt(111) substrate.

I. Introduction

The interaction of chlorine or chlorides with metal surfaces has been a subject of both practical and fundamental scientific interest. Understanding chloride ion behavior on platinum has been important in the electrochemical community, largely due to the role it plays in the kinetics of reactions at fuel cell electrodes.[1−3] Coadsorption of HCl and water on Pt(111) in ultrahigh vacuum (UHV) has been used to infer information about the aqueous/Pt(111) electrochemical interface in the presence of chloride.[4−9] There have also been studies under UHV conditions of Cl_2[10,11] and HCl[4,12] adsorption on Pt(111).

Garwood and Hubbard studied the adsorption and reaction of HCl on Pt(111) in UHV at room temperature.[12] Using temperature programmed desorption (TPD), low energy electron diffraction (LEED), and Auger electron spectroscopy (AES) measurements, they conclude that HCl dissociated on the surface but did not form an ordered layer after an exposure of >400 monolayers (ML) at 300 K. No ordered layer was detected by LEED after subsequent heating. HCl and Cl were found to be the primary desorbing species upon heating above 300 K. Wagner and Moylan studied the adsorption of HCl, alone and with water, on Pt(111) using TPD, LEED, and high resolution electron energy loss spectroscopy (HREELS).[4] They conclude that HCl dissociates upon adsorption at 90 K. This conclusion was supported by (a) the apparent second-order desorption line shape of HCl due to the recombination reaction $H_a + Cl_a \rightarrow HCl_g$, (b) the desorption of a small amount of atomic Cl at high temperature, (c) the desorption of small amounts of H_2, and (d) a shift to lower temperature for HCl desorption after preadsorbing H_2. For HCl exposures of 0.5 langmuirs (L) and greater, they found a sharp (3×3) LEED pattern. The (3×3) LEED pattern has also been observed by others for the dissociation of Cl_2 on Pt(111).[10,11] They also found HREELS evidence for a Pt−Cl stretch but no evidence for an H−Cl stretch. At 90 K, Wagner and Moylan determined a saturation coverage of 0.7 Cl/Pt after a 160 L exposure but were unable to grow multilayer HCl ice because the sublimation rate of bulk HCl is ~2700 ML s^{-1} at 90 K.[13]

More recently, Ito and co-workers have reported studies of HCl, and HCl + water, on Pt(111) using scanning tunneling microscopy (STM) and infrared reflection absorption spectroscopy (IRAS) measurements.[5−8] STM images for HCl adsorption on Pt(111) demonstrate a (3×3) Cl structure with a local coverage of 4/9 Cl/Pt ($\Theta = 0.44$ ML), found after exposure to 1.5 L of HCl at 90 K[7] and in islands after annealing above 160 K.[5] A phase transition from the (3×3) Cl overlayer to a c(4×2) overlayer, with a local coverage of 4/8 Cl/Pt ($\Theta = 0.5$ ML), was found after a 2 L HCl exposure at 90 K.[7] The domain size of the c(4×2) structure was very small, and such structures appeared to cover only part of the imaged region.

There have been no reports of HCl desorption on Pt(111) below 90 K and no observations of molecular adsorption of HCl on Pt(111). In this work, we report TPD and IRAS measurements of HCl deposited on Pt(111) at 20 K using molecular beam techniques. Two distinct peaks and one shoulder are found in the TPD below 90 K and at temperatures above the multilayer desorption ($T > 68$ K). The IRAS measurements indicate that the lower temperature peak at 77 K is due to molecularly adsorbed HCl and has an integrated coverage of 0.22 ML when saturated. The higher temperature feature at 84 K exhibits close to first-order desorption kinetics and saturates at a surface coverage of 0.38 ML. This feature correlates with saturation of the established (3×3) Cl (4/9 Cl/Pt) overlayer observed for both HCl[7] and Cl_2[10,11] adsorption. However, the peak near 84 K does not exhibit the strong adsorbate−adsorbate repulsion found for the higher temperature peaks and we assign

* Corresponding author. Phone: (509) 376-0028. Fax: (509) 376-6066. E-mail: Bruce.Kay@pnl.gov.
[†] Environmental Molecular Sciences Laboratory, Pacific Northwest National Laboratory.
[‡] Fundamental Science Division, Pacific Northwest National Laboratory.
[§] Université de Sherbrooke.

10.1021/jp058139p CCC: $30.25
Published on Web 07/26/2005

this peak to desorption of molecularly bound HCl. Above 100 K, we observe two desorption features that we assign to recombinative desorption of dissociated HCl. A kinetic analysis of the TPD is performed, and for $\Theta < 0.25$, we find a strong repulsive coverage dependence of the desorption energy. The line shape of the HCl spectra at low coverage is similar to that found in other systems with adsorbate−adsorbate repulsion,[14−17] and we conclude such a mechanism is responsible for the strong coverage dependence observed here.

II. Experimental Section

The experiments were performed in an ultrahigh vacuum (UHV) chamber with a base pressure of $\leq 1.0 \times 10^{-10}$ Torr. The sample was a 1 cm diameter, 1 mm thick Pt(111) disk. The sample was spot welded to two tantalum wire leads, 2 mm in diameter, clamped in a Au plated Cu jig attached to a closed cycle He cryostat, and resistively heated through the Ta leads. The temperature was monitored with a K-type thermocouple spot welded to the back of the sample and controlled by computer over a range of 20−1200 K. Temperature calibration was performed using the desorption of multilayers of Ar and N_2[18] and further confirmed using the desorption of H_2O multilayers.[19] The error in the absolute temperature was estimated to be less than ±2 K. The sample was cleaned by repeated cycles of Ne ion sputtering and annealing in O_2 (1.0×10^{-6} Torr, 1000 K, 300 s) and UHV (1150 K, 100 s). The surface purity and order of the Pt(111) substrate were checked using AES and LEED. The cleanliness was confirmed by comparing the monolayer TPD spectra of H_2O and N_2 with reference spectra collected from clean Pt(111) samples under similar conditions. We find this to be a sensitive check for frequently observed background contamination such as CO. Immediately prior to each experiment, the sample was flashed to 1000 K and then cooled to the initial experimental temperature.

The quasi-effusive HCl beam was produced by expanding the neat gas (Matheson > 99.0%) at 2.0 Torr through a 1 mm diameter aperture. The beam was triply differentially pumped prior to impinging on the Pt(111) target. The HCl flux was calculated by determining the flux of Ar at the same backing pressure and correcting for the mass difference. We estimate the uncertainty in the calibration to be ±12%. The HCl beam illuminated the entire face of the sample at 45° with respect to the sample normal with a flux of 0.23 ML s^{-1} relative to the Pt(111) surface (1.51×10^{15} atoms cm^{-2}). All HCl exposures are reported relative to the Pt(111) surface. The King and Wells[20] technique was used to measure the initial sticking coefficient. At 20 K, the initial sticking was greater than 0.9 ± 0.05 and increased monotonically with HCl coverage, reaching unity by 0.45 ML. With a sticking coefficient of ∼1, we take the initial total Cl (HCl + Cl) surface coverage as being equal to the beam fluence, and it will be reported as coverage. Electronically controlled shutters between the second and third differential pumping apertures allowed for control of the relative HCl coverage to better than ±0.02 ML.

The HCl desorption signal was monitored with a quadrupole mass spectrometer located along the sample normal. In a line-of-sight configuration, with a single pass through the ionizer, the mass spectrometer sensitivity is inversely proportional to the velocity of the desorbing species. The HCl ($m/e = 36$) signal is very small when desorbing HCl in the background, so we expect only a small component of the mass spectrometer signal to originate from molecules not in the line-of-sight beam. Therefore, the mass spectrometer signal is corrected for the velocity dependent sensitivity by multiplying by $T^{1/2}$.

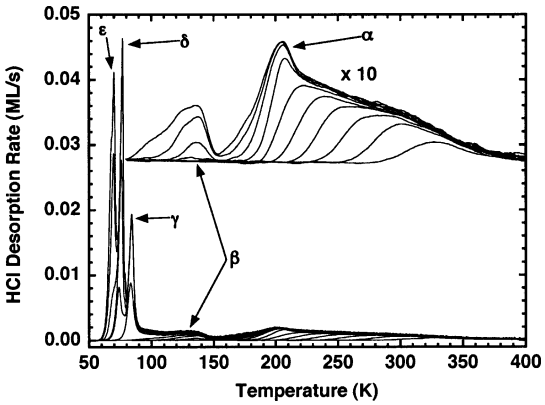

Figure 1. Temperature programmed desorption of HCl ($m/e = 36$) from Pt(111). The HCl was deposited at 20 K and 45° with a flux of 0.23 ML s^{-1} and then heated at a rate of 1.0 K s^{-1}. The initial HCl coverages were 0.02, 0.05, 0.07, 0.09, 0.11, 0.13, 0.15, 0.18, 0.20, 0.22, 0.30, 0.41, 0.49, 0.60, 0.70, and 0.80 ML vs Pt(111). Inset: Ordinate expanded 10× for initial coverages of 0.02−0.22 ML.

Infrared reflection absorption spectra were recorded with a Bruker Equinox 55 Fourier transform spectrometer. The unpolarized infrared beam was focused onto the sample and collected using a pair of BaF_2 lenses ($f = 25$ cm), mounted in a differentially pumped compartment adjacent to the UHV chamber, and isolated with KBr windows. External to the UHV chamber, the infrared signal was focused onto a liquid nitrogen cooled mercury cadmium telluride (MCT) detector using an off axis parabolic mirror ($f = 5$ cm). Data were collected at a sample temperature of 20 K with a resolution of 4 cm^{-1}.

III. Results

Figure 1 displays a set of HCl ($m/e = 36$) coverage dependent TPD spectra for initial HCl coverages between $\Theta = 0.02$ ML and $\Theta = 0.80$ ML using a heating rate of 1 K s^{-1}. The TPD spectra for the ($m/e = 35$) isotope of Cl are not shown but are qualitatively similar to the HCl ($m/e = 36$) spectra. Desorption of molecular HCl from multilayer samples indicates the ($m/e = 35$) signal is predominantly due to cracking in the mass spectrometer. In some experiments, we detected a small increase above the apparent baseline in the ($m/e = 35$) signal starting near 950 K and persisting to 1100 K, but no distinct peak was observed which would correlate with atomic Cl desorption. This is in contrast to the small but well resolved ($m/e = 35$) peak near 960 K reported by Wagner.[4] We found no evidence of desorption for Cl_2 ($m/e = 70$).

The HCl TPD spectra in Figure 1 show a variety of features and span a wide temperature range. We observe five peaks or features prior to the onset of multilayer desorption at ∼68 K that we label in Greek alphabetical order (α, β, γ, δ, and ϵ) from lowest to highest coverage. These peaks fill from high to low temperature as the initial HCl coverage is increased. To facilitate the description of the TPD features, we have summarized the coverage range and peak temperature of the TPD peaks from Figure 1 in Table 1.

The desorption rate for the lower HCl coverages has been scaled by a factor of 10 and is shown as an inset in Figure 1. The TPD spectra for $\Theta \leq 0.20$ ML show a broad peak, labeled α, starting near 380 K which moves to lower temperature with increasing coverage. This peak has coincident trailing edges and a peak desorption rate near 200 K. It spans a temperature range from 160 to ∼380 K. Below 160 K, there is a second peak, labeled β, which fills from the high temperature side with increasing coverage. This peak saturates for $\Theta > 0.25$ ML, and

TABLE 1: Peak Temperatures, Coverage Range, and Adsorbed State for HCl Desorption from Pt(111) (the Entries in Parentheses Are Tentative Assignments)

peak label	coverage range (ML)	peak or range (K)	adsorbed state
α	0−0.20	200	dissociated
β	0.20−0.25	100−160	(dissociated)
γ	0.25−0.38	84	(molecular)
δ	0.38−0.60	77	molecular
ϵ	0.60−0.76	70	molecular
multilayer	0.76−	<68	molecular

once saturated, the desorption rate varies by only about 20% from the minimum near 110 K to the broad maximum at ~135 K. Below 90 K, there are three sharp peaks (γ, δ, and ϵ) in the TPD spectrum which fill sequentially with increasing initial HCl coverage. The highest temperature peak in this region, γ, has a peak desorption rate near 84 K. In contrast to the lower coverage α and β peaks, the γ peak fills relatively symmetrically with increasing coverage and saturates for $\Theta \geq 0.38$ ML. At lower temperature, the δ peak fills with nearly coincident leading edges and has a peak desorption rate near 77 K when saturated for $\Theta \geq 0.60$ ML. The final peak, ϵ, has a peak desorption rate near 70 K. The ϵ peak is not well separated from the multilayer bulk desorption, which can be seen as the small shoulder on the low temperature side of the highest coverage spectra shown, $\Theta = 0.80$ ML. The overlap with the multilayer desorption makes the determination of the saturation coverage and filling order difficult, but we estimate the saturation coverage to be close to ~0.76 ML and the filling to be close to exhibiting coincident leading edges. For all initial exposures, $\Theta \geq 0.80$ ML (data not shown), the leading edges coincide and zero-order desorption from bulk HCl results. The α peak and the high temperature side of the β peak were reported previously by Wagner.[4] The lower temperature desorption features γ, δ, and ϵ have not been reported before.

The TPD spectra in Figure 1 exhibit a broad range of features. The three lowest temperature peaks (γ, δ, and ϵ) are narrow with a ΔT (fwhm)/T value of ~0.1, while the high temperature peaks are broad ($\Delta T/T$ for β is ~0.5, and $\Delta T/T$ for α is ~1). The lowest temperature peaks (δ and ϵ) fill with coincident leading edges characteristic of zero-order desorption kinetics. The γ peak fills nearly symmetrically, close to the self-similar filling behavior resulting from first-order desorption kinetics with constant desorption energy. The β and α peaks fill with coincident trailing edges. This behavior can result from a wide distribution of adsorbate binding sites, strongly repulsive adsorbate−adsorbate interactions, second-order desorption kinetics, or some combination of these conditions. It would be unlikely that Pt(111) would have a broad distribution of binding sites for HCl because it does not exhibit this behavior for other small molecules and atoms such as N_2, Ar, and H_2O. Recombination of dissociated HCl would result in second-order desorption kinetics, but the width of the α peak suggests that there is a significant variation in desorption energy in the low coverage region in addition to a possible second-order desorption mechanism.

To estimate the energy dependence of the desorption kinetics for the spectra shown in Figure 1, we performed an analysis using the Polanyi−Wigner equation:[21]

$$-\frac{d\Theta}{dt} = \nu(\Theta)\exp[-E(\Theta)/RT]\Theta^n \qquad (1)$$

where Θ is the adsorbate coverage, n is the desorption order, t is time, ν is the preexponential factor for desorption, $E(\Theta)$ is the coverage dependent desorption energy, R is the universal gas constant, and T is the temperature. Temperature and time are related by the heating rate, β, where $\beta = dT/dt$, which was 1 K s^{-1} in our experiments. Equation 1 is solved for $E(\Theta)$ assuming a coverage independent preexponential factor, which is varied to achieve self-consistency in the calculated $E(\Theta)$ for different initial coverages. The procedure has been discussed in greater detail in previous work.[22] We find relatively good agreement between an individual $E(\Theta)$ expression and the experimental data over a range of preexponential factors from about 1.0×10^{12} to 5.0×10^{14} ML^{1-n} s^{-1}.

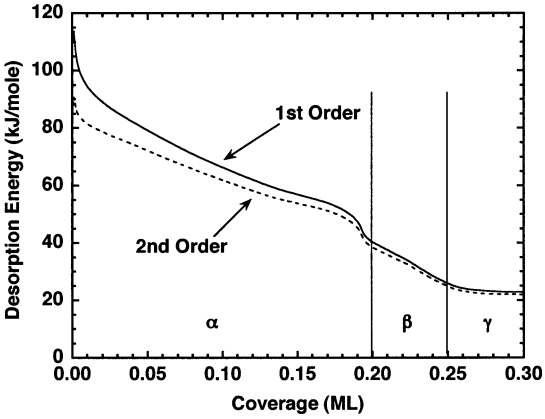

Figure 2. Activation energy for desorption of HCl from Pt(111) as a function of HCl coverage, shown for $\Theta < 0.3$ ML. The data are the inversion of a single TPD experiment using the Polanyi−Wigner equation with a preexponential factor of 10^{13} ML^{1-n} s^{-1} assuming first-order (solid line) and second-order (dashed line) kinetics. The corresponding coverage ranges for the α, β, and γ TPD peaks are indicated.

Figure 2 shows a pair of $E(\Theta)$ curves calculated from the data in Figure 1 using the same numerical value for the preexponential factor, 1.0×10^{13} ML^{1-n} s^{-1}, and assuming a desorption order of one and two. The figure shows the $E(\Theta)$ curves corresponding to the lower coverage region of the TPD spectra in Figure 1, $\Theta < 0.30$ ML. The line shape of the TPD spectra in Figure 1 for $\Theta < 0.30$ ML makes a zero-order desorption mechanism unlikely, and thus, only the calculations from first- and second-order kinetics are shown. Different peaks in the TPD spectra can have different kinetic orders and different preexponential factors, and this analysis is not intended to be a detailed kinetic description. Rather, the purpose is to point out relative differences in desorption energy as a function of coverage. The lowest coverage range in the $E(\Theta)$ curve corresponds to desorption from the α peak in Figure 1. In this coverage range, desorption energy decreases dramatically with increasing coverage. There is a sharp decrease in $E(\Theta)$ near $\Theta = 0.20$ ML, and above this coverage, the $E(\Theta)$ curve corresponds to desorption from the β peak. The $E(\Theta)$ curves for $\Theta > 0.25$ ML are not strongly coverage dependent, and this region corresponds to desorption from the γ peak. The full $E(\Theta)$ range of the γ peak is shown in Figure 3.

The $E(\Theta)$ curves in Figure 2 show that, using either first- or second-order desorption kinetics, there is a large variation in the apparent desorption energy as a function of coverage for $\Theta \leq 0.25$ ML. At low coverage, the calculations for $E(\Theta)$ assuming different kinetic orders will show the greatest differences, with a lower $E(\Theta)$ resulting from higher kinetic order. However, even with second-order desorption kinetics, the α and β peaks show a large decrease in $E(\Theta)$ as the coverage increases. Using the first-order $E(\Theta)$ curve, the desorption energy for the α peak decreases from 90 kJ mol^{-1} at $\Theta = 0.02$ ML to 50 kJ mol^{-1} when saturated near $\Theta = 0.20$ ML, a factor of 1.8

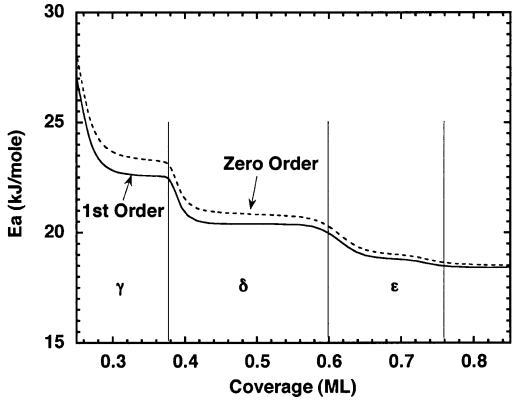

Figure 3. Activation energy for desorption of HCl from Pt(111) as a function of HCl coverage shown for $\Theta \geq 0.25$ ML. The data are the inversion of a single TPD experiment using the Polanyi−Wigner equation with a preexponential factor of 10^{13} ML^{1-n} s^{-1} assuming zero-order (dashed line) and first-order (solid line) kinetics. The corresponding coverage ranges for the γ, δ, and ϵ TPD peaks are indicated.

decrease. The β peak desorption energy decreases from 50 kJ mol^{-1} at $\Theta = 0.20$ ML to 25 kJ mol^{-1} when saturated near $\Theta = 0.25$ ML, a factor of 2 decrease. It is clear from the $E(\Theta)$ data in Figure 2 that a coverage independent second-order desorption model will not describe the data in Figure 1 for the α and β peaks.

Figure 3 shows a pair of $E(\Theta)$ curves calculated from the data in Figure 1 that includes the higher coverage peaks in the TPD spectrum, $\Theta > 0.25$ ML. The manner in which the higher coverage peaks (γ, δ, and ϵ) fill suggests the appropriate desorption kinetics will be either zero or first order and these are the $E(\Theta)$ curves shown. The same preexponential factor has been used, 1.0×10^{13} ML^{1-n} s^{-1}. The shapes of the $E(\Theta)$ curves are quite different from those shown in Figure 2. There are two plateaus in the $E(\Theta)$ curves with close to constant desorption energy prior to reaching the constant $E(\Theta)$ resulting from multilayer bulk desorption. The first of these, at lower coverage, corresponds to the γ peak and has a first-order desorption energy of 22.6 kJ mol^{-1}. The plateau region for the γ peak extends from about $\Theta = 0.30$ ML to $\Theta = 0.38$ ML. The second plateau corresponds to desorption from the δ peak and has a first-order desorption energy of 20.4 kJ mol^{-1}. This plateau extends from about $\Theta = 0.42$ ML to $\Theta = 0.58$ ML. The width of the plateau associated with the δ peak, 0.16 ML, is twice that of that associated with the γ peak. There is no clear flat region in the $E(\Theta)$ curve associated with the ϵ peak but rather a gentle decrease from the end of the δ peak region to the final constant $E(\Theta)$ value resulting from bulk desorption. The middle point in coverage for the ϵ peak, $\Theta = 0.66$ ML, has a first-order desorption energy of 18.7 kJ mol^{-1}. This is only about 0.2 kJ mol^{-1} greater than the bulk desorption energy. The difference in energy is about the same for a comparison using the zero-order $E(\Theta)$ curve.

For $\Theta > 0.76$, $E(\Theta)$ is constant (zero order, 18.5 kJ mol^{-1}) and represents the desorption energy of bulk HCl. A calculation of the desorption energy from vapor pressure data,[13] assuming a HCl surface density of 7.3×10^{14} molecules cm^{-2}, yields an activation energy of 19.7 kJ mol^{-1} with a preexponential factor of 4.8×10^{14} ML s^{-1}. The desorption rate calculated from the vapor pressure data differs from the rate calculated using the experimentally determined kinetics by less than a factor of 2 from 54 to 90 K. We consider this level of agreement to be acceptable and well within the uncertainties introduced from the absolute temperature calibration and the assumed HCl density.

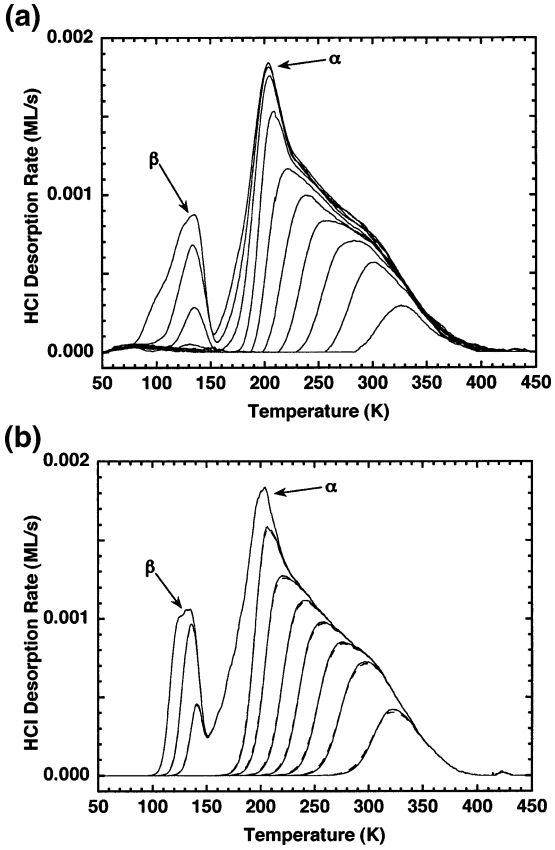

Figure 4. (a) Temperature programmed desorption of HCl (m/e = 36) from Pt(111). The HCl was deposited at 20 K and 45° with a flux of 0.23 ML s^{-1} and then heated at a rate of 1.0 K s^{-1}. The initial HCl coverages were 0.02, 0.05, 0.07, 0.09, 0.11, 0.13, 0.15, 0.18, 0.20, and 0.22 ML vs Pt(111). (b) Simulated HCl TPD spectra using the first-order (solid lines) and second-order (dashed lines) kinetic parameters shown in Figure 2. The initial coverages used in the simulation are the same as the experimental data in part a. The α and β TPD peaks are labeled.

Figure 4a shows a set of low coverage TPD data similar to that shown in Figure 1, and Figure 4b shows simulated spectra, obtained by numerical integration of the Polanyi−Wigner equation using the $E(\Theta)$ curves shown in Figure 2, for the same initial values of Θ as those in Figure 4a. The simulations are shown for both first- and second-order kinetics, and the difference between the two is small. The agreement between the simulated spectra and the experimental data is good for all initial coverages. This level of agreement using a single $E(\Theta)$ curve for each kinetic order results only if the preexponential factor is a reasonable approximation to the correct value. The agreement lends support to using the $E(\Theta)$ curves as a measure of relative changes in desorption energy. The small differences between TPD curves simulated for different reaction orders demonstrate that even using the complete data set in the analysis does not allow the reaction order to be unambiguously assigned without additional data.

Figure 5a shows a selection of the higher coverage data from Figure 1. This shows clearly the three peaks in the low temperature desorption of HCl. The multilayer desorption peak grows in as a low temperature shoulder on the ϵ peak for $\Theta = 0.8$. Figure 5b shows simulated spectra calculated using the $E(\Theta)$ curves in Figure 3. The simulations are shown for both zero- and first-order desorption kinetics, and again, the difference between the two is small. The agreement between the experimental data and the simulated TPD spectra at all coverages is

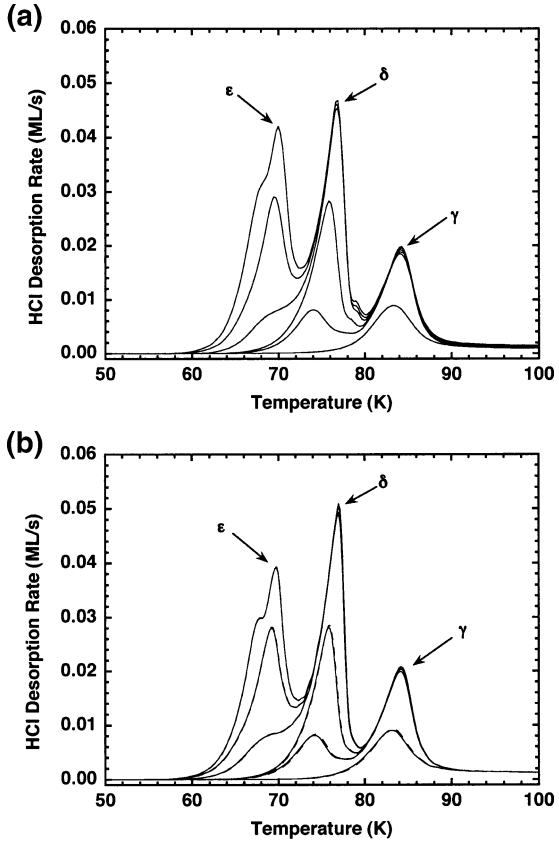

Figure 5. (a) Temperature programmed desorption of HCl (m/e = 36) from Pt(111). The HCl was deposited at 20 K and 45° with a flux of 0.23 ML s^{-1} and then heated at a rate of 1.0 K s^{-1}. The initial HCl coverages were 0.30, 0.41, 0.49, 0.60, 0.70, and 0.80 ML vs Pt(111). (b) Simulated HCl TPD spectra using the first-order (solid lines) and zero-order (dashed lines) kinetic parameters shown in Figure 3. The initial coverages used in the simulation are the same as the experimental data in part a. The γ, δ, and ϵ TPD peaks are labeled.

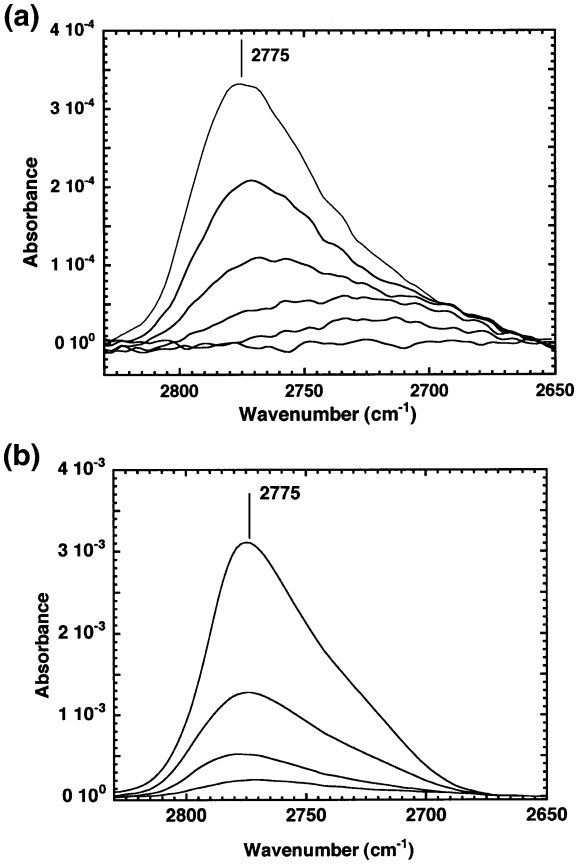

Figure 6. IRAS spectra of HCl deposited on Pt(111) at 20 K. The spectra were recorded at 20 K, and each is the average of 3200 interferograms. HCl coverage: (a) 0.20, 0.28, 0.37, 0.46, 0.55, and 0.64 ML; (b) 0.55, 0.74, 1.00, and 1.56 ML. The data have been baseline corrected using a linear baseline subtraction intersecting the data near 2650 and 2900 cm^{-1}.

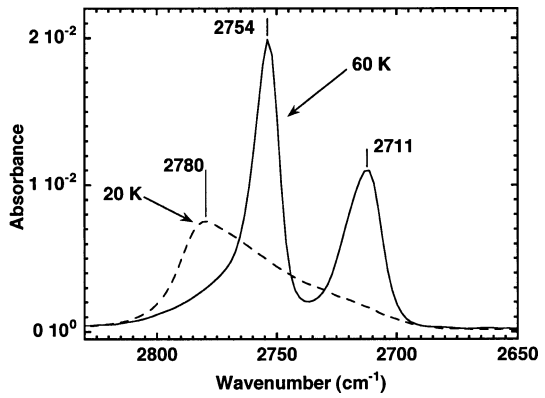

Figure 7. IRAS spectra of 3.5 ML of HCl deposited on Pt(111) at 20 K and subsequently heated at 0.1 K s^{-1}. The spectra shown were recorded at 20 K (dashed line) and 60 K (solid line).

good and supports accepting the calculated desorption energies as approximately correct.

Figure 6a shows IRAS spectra of HCl adsorbed on Pt(111) at 20 K for a sequence of initial exposures from $\Theta = 0.20$ ML to $\Theta = 0.64$ ML, and Figure 6b shows a similar sequence with initial exposures spanning $\Theta = 0.55-1.56$ ML. The raw spectra exhibited substantial variations in the baseline with increasing coverage, and the data presented have had a linear baseline subtracted from it. The two highest coverage spectra in Figure 6a, $\Theta \geq 0.46$, and all of the spectra in Figure 6b show a broad absorption centered near 2775 cm^{-1}. This is the only absorption feature found in the experimentally accessible wavelength range, which extends from about 1200 to 3800 cm^{-1}. This absorption band is in the region expected for the H−Cl stretch observed in crystalline HCl, although the absorption peak is blue shifted from that reported for crystalline HCl at 73 K.[23] The lowest temperature phase of crystalline HCl has been reported with two strong absorptions at 2704 and 2744 cm^{-1}.[23] The absorption near 2775 cm^{-1} observed for $\Theta \geq 0.46$ spans the range of the two bands observed in crystalline HCl.[23] A broad absorption instead of the sharp peaks reported for bulk crystalline samples is consistent with the adsorbed HCl being amorphous. Further confirmation of this assignment comes from HCl crystallization experiments on thicker (2−100 ML) samples.

Figure 7 shows two spectra from an HCl crystallization experiment. The Pt(111) substrate was exposed to 3.5 ML of HCl at 20 K and then heated at 0.1 K s^{-1} to 60 K while recording IRAS spectra as a function of temperature. For clarity, only two spectra are shown. The initial spectrum recorded at 20 K shows a broad absorption centered near 2775 cm^{-1}. Upon heating, the IR spectrum evolves into two sharp peaks at 2711 and 2754 cm^{-1} slightly blue shifted from the reported bulk crystalline peaks at 73 K,[23] and we interpret the spectrum at 60 K as resulting from crystalline HCl. We only observe these bands for coverages that are greater than 1 ML. For coverages between 0.28 and 0.50 ML deposited at 55 K (data not shown), we observe an FTIR line shape that is nearly the same as the line shape for spectra deposited at 20 K. The dramatic change in the spectra in Figure 7 between 20 and 60 K and the agreement between the reported bulk crystalline HCl spectra[23]

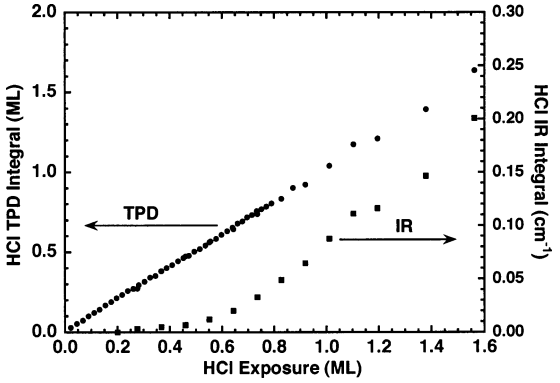

Figure 8. Integrated HCl desorption vs initial HCl coverage (solid circles) and integrated IR absorbance between 2650 and 2850 cm^{-1} for HCl deposition at 20 K (solid squares).

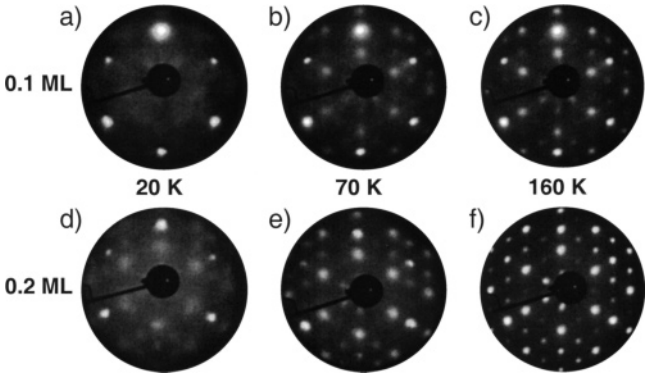

Figure 9. LEED images of HCl adsorbed on Pt(111) at 20 K as a function of annealing temperature. The HCl was deposited at 20 K, and the initial coverage was 0.1 ML (a−c) and 0.2 ML (d−f). Images a and d are as deposited, images b and e are after annealing to 70 K, and images c and f are after annealing to 160 K.

and the 3.5 ML sample at 60 K support the assignment of the 20 K spectra in Figures 6 and 7 as resulting from an amorphous HCl structure.

The lowest coverage spectrum in Figure 6a is $\Theta = 0.20$, and this spectrum is essentially flat, showing no observable HCl stretch. The same result was obtained for all coverages less than 0.20 ML. The next two spectra in Figure 6a, $\Theta = 0.28$ and 0.37 ML, have an apparent absorption which is slightly red shifted from the higher coverage spectra. Even though these spectra have peaks that are slightly red shifted from the higher coverage spectra, we also interpret these peaks as resulting from the molecular HCl stretch. This assignment, however, is less certain because of the small signal intensity and the dramatic curvature of the baseline in this region. The spectrum for $\Theta =$ 0.46 ML has a line shape similar to the higher coverage spectra, and we interpret this as being clearly due to an HCl stretch IR absorption.

Figure 8 shows the integrals of TPD spectra similar to those shown in Figure 1 and of the 2775 cm^{-1} band between 2650 and 2850 cm^{-1} of the IR spectra in Figure 6 as a function of the initial HCl coverage. The TPD integrals shown in Figure 8 are linear over the entire coverage range. For $\Theta \geq 0.76$ ML, desorption results from bulk sublimation where molecular HCl is expected to be the only desorbing species. Because the integrated desorption remains linear down to low initial coverage, we conclude that molecular HCl is the primary desorbing species at all coverages. Both Wagner[4] and Garwood[12] determined a small fraction of the adsorbed HCl desorbed as H_2 near 350 K and Cl atoms near 950 K. Wagner determined the H_2 coverage after a 1.8 L HCl (0.4 ML) exposure was about 5% of the saturation coverage of H_2 on Pt(111). We detected a small amount of H_2 ($m/e = 2$) near 350 K but also found a much larger signal when desorbing multilayer HCl, making it difficult to separate H_2 desorption from the surface from reaction in the mass spectrometer. We found no resolvable peak for Cl ($m/e = 35$) up to 1100 K but did observe a rise above the baseline for $T > 950$ K. Appreciable desorption of some HCl by the competing H_2 and Cl channels would result in a nonlinearity in the low coverage region of the TPD integrals, which we do not observe. From our data, we estimate an upper bound of 10% desorbing by channels other than molecular HCl. There are two possible reasons why we do not detect the desorption of atomic Cl observed in the earlier study.[4] One is that the ($m/e = 35$) background in our mass spectrometer may be large enough to obscure the small atomic Cl desorption peak. Desorption of molecular HCl always resulted in the appearance of a ($m/e =$ 35) background with a long (>1000 s) time constant. The second is that recombination with background hydrogen during the TPD could reduce the amount of atomic Cl available for desorption at $T > 950$ K. Regardless of the reason for the difference, our data support molecular HCl as the primary desorbing species, and this agrees with the earlier study by Wagner.[4]

In contrast to the TPD integrals, the integrals of the IR absorption in the H−Cl stretch region shown in Figure 8 are not linear and the zero absorption intercept is shifted to higher coverage. They appear to be close to linear for $\Theta \geq 0.64$ ML but show absorbance at lower coverage than the intercept of a linear extrapolation of the higher coverage data. The spectra for $\Theta \geq 0.46$ ML show an H−Cl stretch IR absorption, but the integrated absorbance is nonlinear with respect to the higher coverage data. Because of the surface selection rule for IRAS, it is not possible to discriminate between molecular orientation effects and dissociation giving rise to an absence of IR absorption at low coverage. These data suggest that the upper limit for the saturation coverage of dissociated HCl on Pt(111) is close to $\Theta = 0.44$ ML (4/9 Cl/Pt). However, on the basis of the TPD data discussed below, HCl appears to be molecularly adsorbed for $\Theta \geq 0.38$ ML and is probably molecular for $\Theta \geq$ 0.25 ML.

Long range order of the Cl overlayer was monitored by LEED for different initial HCl coverages as a function of annealing temperature. The samples were heated to a designated temperature and then immediately cooled to 20 K where the LEED spectra were obtained. Figure 9a−c displays a sequence of LEED images taken after depositing 0.1 ML of HCl at 20 K on the Pt(111) surface. After initial exposure, only the spots from the Pt(111) substrate are observed. After heating the sample to 70 K, a weak (3×3) LEED pattern is observed. This pattern has a greater intensity at the points that result from a (3×3) structure with 4/9 Cl/Pt coverage. In the remaining discussion, we refer to this pattern as (1.5×1.5) in contrast with the simple 1/9 Cl/Pt (3×3) overlayer. A schematic of these overlayer structures and the corresponding LEED patterns are shown in Figure 10. The positions of the Cl atoms are based on published STM data.[5,7] The LEED pattern continues to sharpen after heating to 100 K (data not shown) and 160 K, shown in Figure 9c. The intensity of the overlayer pattern decreases after heating to 200 K and disappears after heating to 300 K (data not shown). Figure 9d−f displays a similar sequence of LEED images taken after an initial exposure of 0.2 ML at 20 K. For this initial coverage, a diffuse (1.5×1.5) pattern with considerable background intensity is observed before heating the sample. It sharpens when annealed to 70 K (Figure 9e), and here, the spots of a simple (3×3) LEED pattern are also evident. The LEED

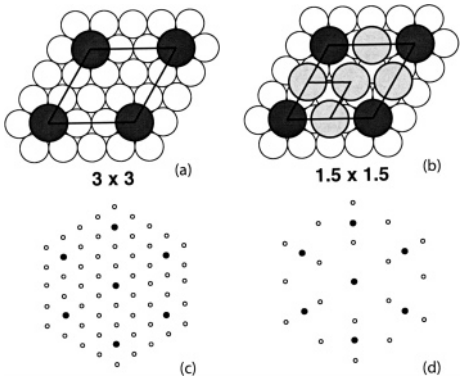

Figure 10. Real space and reciprocal space images of (3 × 3)[1/9] (a,c) and (3 × 3)[4/9] (b,d) overlayers on a Pt(111) surface. The open circles are atoms in the Pt(111) substrate. The filled circles are the adatoms. The dark gray filled circles are located on atop sites relative to the Pt(111) substrate, and the light gray filled circles are located on bridge sites of the Pt(111) substrate. The relative size of the circles is proportional to their relative size (1.37 Å for Pt and 1.81 Å for Cl^-). The positions of the Cl atoms are based on published STM data.[5,7]

pattern sharpens further after heating to 160 K (Figure 9f), with the intensity in the (1.5 × 1.5) spots greater than the spots unique to the simple (3 × 3) pattern. As was seen with the 0.1 ML HCl exposure, the LEED patterns for the 0.2 ML exposure are weaker after heating to 200 K and disappear after heating to 300 K (data not shown). Experiments with initial exposures of 0.4 and 0.6 ML HCl were also performed (data not shown). The initial (no heating) LEED patterns for these coverages consist of both the simple (3 × 3) and (1.5 × 1.5) overlayer structures but with increased background intensity. Upon heating, these LEED patterns follow a similar trend to the 0.1 and 0.2 ML exposure data, that is, sharpening after heating to 160 K and disappearing by 300 K. Although the LEED data shown in Figure 9 and described above were obtained at 20 K, we did monitor the LEED intensity during heating and cooling. For all HCl exposures, we observed that the LEED pattern disappeared after heating above 200 K and would reemerge after the sample had cooled below 180 K. A similar observation has been reported for HCl on Pd(111), and the effect has been ascribed to an order−disorder transition.[24]

Previous studies have agreed that Cl from Cl_2 or HCl forms (3 × 3) LEED patterns on Pt(111).[4,10,11] However, the reported saturation coverage has ranged from $\Theta = 0.2$ ML to $\Theta = 0.5$ ML. The simple (3 × 3) structure, shown in Figure 10a, would have a saturation coverage of 1/9 Cl/Pt which is lower than what has been reported.[4,10] There are a number of ways that higher Cl/Pt ratios can be achieved which are commensurate with the Pt(111) lattice with a (3 × 3) periodicity. A (1.5 × 1.5) LEED pattern is a subset of the simple (3 × 3)[1/9] pattern, and a superposition of the two patterns would appear spatially identical to the (3 × 3) pattern. The STM study by Fukushima et al.[5] reports that islands of the (1.5 × 1.5)[4/9] structure were observed at low coverage. In contrast, Cl_2 adsorbed on Pt(111) at 300 K only exhibits a (3 × 3) LEED pattern for Θ between 0.45 and 0.56 ML.[10] We find that after heating to 70 K the LEED patterns have spots corresponding to the (3 × 3) overlayer structure but with greater intensity at the points corresponding to the (1.5 × 1.5) overlayer structure. The TPD results shown in Figure 5a indicate that after heating to 70 K most of any initial HCl deposition less than $\Theta = 0.44$ ML (4/9 Cl/Pt) would remain on the Pt(111) sample. Although not quantitative, the greater intensity at the points in the LEED pattern corresponding to the (1.5 × 1.5) overlayer structure shown in Figure 9 suggests that that some fraction of the HCl is clustered into ordered islands with a 4/9 Cl/Pt local coverage. Heating to 70 K presumably allows adsorbed HCl to diffuse on the Pt(111) surface and results in growth and ordering of the islands with respect to the Pt(111) surface.

IV. Discussion

The HCl TPD spectra in Figure 1 show five distinguishable desorption features prior to the onset of bulk multilayer desorption. The features are labeled in Figure 1, and the coverage ranges and peak desorption temperatures for each feature are summarized in Table 1. Also listed in Table 1 is our assignment of whether the desorption feature is from dissociated or molecular HCl. In the following discussion, we consider the TPD features from low to high coverage and discuss the basis for these assignments.

The lowest coverage feature, labeled α, has a coverage range from 0 to 0.20 ML and a saturation peak desorption temperature at 200 K. The temperature width of the α peak, the coincidence of the trailing edges, and the peak shift to lower temperatures with increasing coverage are all suggestive of repulsive adsorbate−adsorbate interactions. The coverage dependence of the TPD line shapes is similar to that of many other molecules with repulsive desorption line shapes (e.g., NH_3 on Au(111),[14] O_2 on Ru(0001),[15] and CH_3Cl on Cu(110)[16] and Ru(001)[17]). The kinetic analysis shown in Figure 2 confirms that the desorption energy has a strong repulsive coverage dependence. However, the analysis yields similar results assuming either a first-order ($n = 1$) or a second-order ($n = 2$) desorption mechanism and therefore does not provide unambiguous support for either molecular desorption ($n = 1$) or recombinative desorption from dissociated HCl ($n = 2$).

The primary argument from our data supporting our assignment of the α peak to recombinative desorption from dissociated HCl is the relatively high desorption temperature. In general, the desorption temperature (desorption energy) of a physisorbed species from a metal surface increases with the polarizability and dipole moment of the adsorbate. Comparison of the HCl desorption temperature in the α peak with the desorption temperature of CH_3Cl, which desorbs molecularly, is instructive. The polarizability and dipole moment of CH_3Cl are about 1.0×10^{-23} cm^3 and 2 D,[16,17] whereas the polarizability and dipole moment of HCl are 2.6×10^{-24} cm^3 [25] and 1.1 D.[26] On Pt(111), CH_3Cl desorbs near 145 K,[27] and therefore, on the basis of the smaller dipole moment and polarizability of HCl, we would expect undissociated HCl to desorb below 145 K instead of at 200 K. The desorption temperature of the α peak is therefore consistent with recombinative desorption of dissociated HCl.

This assignment is also consistent with the conclusion of Wagner et al. who studied the adsorption of HCl on Pt(111) at $T > 90$ K using TPD and HREELS data.[4] In that work, the TPD data supporting dissociated HCl at this coverage come from hydrogen preadsorption studies on the Pt(111) substrate. Wagner et al. observed that the TPD spectra resulting from a subsaturation HCl exposure shift to lower temperature with increasing hydrogen exposure, thus supporting a second-order, $H_a + Cl_a \rightarrow HCl_g$, recombination mechanism. Additional support comes from simulating TPD spectra using the $E(\Theta)$ curves from Figure 2 of our study with a heating rate of 10 K s^{-1} used by Wagner et al. A simulation assuming second-order desorption yields a peak desorption rate at 219 K, close to the reported 220 K.[4] In contrast, a first-order simulation shifts the temperature of maximum desorption to 214 K. In the same study, no evidence was found for a molecular H−Cl stretch using HREELS, but there was evidence of a Pt−Cl stretch.[4] It was argued that even

if molecular HCl were lying parallel to the Pt(111) surface some signal should be detected through an impact scattering mechanism. These results support the conclusion that HCl on Pt(111) for $\Theta < 0.2$ ML and $T \geq 90$ K is dissociated. Therefore, the repulsive interaction giving rise to the large coverage dependence of the desorption energy must arise from interatomic rather than intermolecular forces. Because of the high electronegativity of Cl, we expect it to carry at least a partial negative charge and the resulting repulsion to be primarily Coulombic.

While the above arguments support the interpretation that at low coverage ($\Theta < 0.2$ ML) HCl on Pt(111) is dissociated, because the desorption of the dissociated molecule does not begin until about 160 K, it is not clear at what temperature the dissociation occurs. The HREELS data[4] described above were obtained for HCl deposited at 90 K which puts an upper bound on the dissociation temperature. In our experiments, the infrared spectra of 0.2 ML of HCl deposited at 20 K in Figures 6 and 8 show no observable H−Cl stretch. The lack of absorbance for the H−Cl stretch could mean that HCl has dissociated at this temperature, or it could mean that the HCl molecule is adsorbed parallel to the Pt(111) surface and is IR inactive due to the surface selection rule. If HCl has dissociated at 20 K, then on the basis of the TPD desorption energy coverage dependence, we would expect the interactions between the dissociated molecules to be repulsive. However, a replusive interaction at this temperature is at odds with the LEED data presented in Figures 9 and 10 and with the STM data of Ito and coworkers.[5−7] The LEED data suggest that, at low coverage and after annealing above 70 K, HCl clusters into 2D islands with a (1.5×1.5) pattern that results from the local structure of 4/9 Cl/Pt shown in Figure 10b. Similarly, the same local structure of 4/9 Cl/Pt at a low total coverage of HCl has been observed by STM.[5] One explanation of the observed attractive behavior at low temperature (clustering) and the repulsive interactions at high temperature (repulsive coverage dependent desorption energy) is that HCl adsorbs molecularly at low temperature, clusters as the sample is heated, and then dissociates at a temperature below 90 K. Once dissociated, the barrier for diffusion of Cl on Pt(111) is sufficiently high that the 4/9 Cl/Pt local coverage is retained even after heating. In this scenario, the intermolecular potential would be attractive at low temperature due to the interaction of the molecular dipoles. At higher temperatures, after HCl has dissociated, the intermolecular (interatomic) potential would become repulsive due to the negative charge on the Cl atoms. While this mechanism can account for the experimental observations, further low temperature and coverage STM studies would be needed to completely address this issue.

The next feature in the TPD spectra in Figure 1 is β, and it occurs over a coverage range from 0.20 to 0.25 ML and over a broad temperature range from 100 to 160 K. Similar broad features are sometimes found for physisorbed molecules as a result of an increase in the chemical potential, as adsorbed molecules cause compression of the monolayer before growth of the second layer.[28] In the present case, this feature occurs at a coverage (~0.25 ML) where compression is unlikely and at temperatures where HCl is thought to be dissociated.[4] The broad temperature range is also consistent with a picture in which the lowering in energy resulting from dissociation competes against the repulsion between adsorbed Cl. As discussed above, molecular, undissociated HCl would be expected to desorb below 145 K and the high temperature limit of the β peak is at ~160 K. The repulsive character of the TPD peak, shown in Figure 2, compared to the dissociated and repulsive α peak also supports dissociation. We conclude that the adsorbed HCl corresponding to desorption from the β peak is dissociated.

The next peak at higher coverage in the TPD spectra in Figure 1, γ, has a maximum desorption rate near 84 K and the coverage range 0.25 ML $\leq \Theta \leq$ 0.38 ML. With increasing exposure, this peak fills symmetrically, consistent with a first-order desorption mechanism. The saturation of this feature near $\Theta =$ 0.38 ML is close to the 4/9 Cl/Pt ($\Theta = 0.44$ ML) coverage found locally for HCl on Pt(111) by STM which was attributed to dissociated HCl.[6] Similar STM studies, with HCl exposure and imaging at 90 K, referred to the adsorbate as chlorine or chloride.[7] On the other hand, from our TPD studies, the low peak temperature (84 K), the peak shape (first order), and the fairly uniform desorption energy determined in the kinetic analysis shown in Figure 3 suggest a different desorption mechanism from that responsible for the α and β peaks. The desorption features of the γ peak are consistent with being HCl molecularly adsorbed on the Pt(111) surface. This assignment is supported by the onset of a molecular H−Cl stretch for the $\Theta = 0.28$ and 0.37 ML IRAS spectra in Figure 6a. The near uniform desorption energy, ~23 kJ mol^{-1}, over most of the coverage range corresponding to desorption from the γ peak also indicates an absence of adsorbate−adsorbate repulsion as found for the α peak. On the basis of the differences in the desorption behavior of this peak with the α and β peaks (dissociated), we assign desorption from the γ peak as resulting from molecularly adsorbed HCl. Also, given that the saturation of this feature ($\Theta = 0.38$ ML) is close to the 4/9 Cl/Pt ($\Theta =$ 0.44 ML) coverage shown in Figure 10b to saturate the Pt surface, it is likely that this HCl is adjacent to the Pt(111) surface.

The next TPD feature is the near zero-order desorption peak at 77 K, δ, which occurs over the coverage range from 0.38 to 0.60 ML. The ~10 K separation from the multilayer desorption indicates that the HCl that desorbs in this peak has a stronger interaction with the Pt substrate, or the adsorbed HCl layer, than does multilayer HCl. The IRAS spectra in Figures 6 and 8 show that there is a clear molecular stretch absorption in this coverage range. The saturation coverage of this peak is 0.6 ML, and while it is possible to pack this many Cl atoms into a single layer with the van der Waals radius of Cl (1.8 Å) or Cl^- (1.81 Å),[4] such dense packing would likely result in a highly repulsive desorption energy dependence which we do not observe (see Figure 3). A packing density of 0.6 ML for Cl on Pt(111) has been observed in an electrochemical environment[3] and in an UHV experiment by exposure to Cl_2 near 500 K,[10] but in neither case was an ordered layer observed. In the present study, we observed sharp LEED patterns with the same (3×3) or (1.5×1.5) structures as those shown in Figure 9 even after exposure to 0.6 or 10 ML of HCl at 20 K. In the 0.6 ML case, a dense packed overlayer of Cl would not be in registry with the Pt(111) surface, and in the 10 ML case, a sharp LEED pattern can only result from substantial electron stimulated desorption (ESD) of molecular HCl. These observations suggest that molecular HCl not in direct contact with the Pt surface is readily desorbed by ESD, including part of an initial 0.6 ML overlayer. For these reasons, we assign this desorption feature to molecular HCl that is adsorbed in the second layer. The amount of HCl in the δ peak is about 0.22 ML or ~2/9 Cl/Pt. If we consider that the first HCl layer has the Cl structure shown in Figure 10b, as suggested by STM and LEED, then a second layer of HCl adsorbed in the 3-fold hollow sites that are directly centered

over a Pt atom is a possible structure with a saturation coverage of about 2/9 Cl/Pt.

The multilayer desorption grows in as a low temperature shoulder on the ϵ peak with increasing exposure. The ϵ peak indicates the interaction with the Pt substrate extends to coverages near 0.76 ML. This coverage is lower than would be expected for saturation of the second layer. If the second layer retained the density of the first layer, 4/9 Cl/Pt (0.44 ML), then the second layer would saturate at 8/9 Cl/Pt (0.88 ML). Our crystallization studies on thicker films of HCl suggest that multilayer HCl at the temperature of desorption (55 K) is crystalline. The second layer may be a transitional layer between the partially dissociated layer on and close to the Pt(111) surface and the bulk crystalline HCl structure. The ϵ peak might result from restructuring or relaxation of part of the second layer after desorption of a crystalline overlayer. For $\Theta > 0.8$, we observe desorption consistent with bulk sublimation of crystalline HCl.

V. Conclusions

We have investigated the adsorption and desorption of HCl on Pt(111) up through the growth of HCl multilayers. For HCl coverages of $\Theta \leq 0.25$ ML, the observed TPD results from recombinative desorption of HCl dissociated on the Pt(111) surface. The broad desorption temperature range is the result of repulsive interactions, presumably between the dissociated components. The repulsive behavior exhibited in the TPD spectra for temperatures > 100 K contrasts with the clustering indicated by LEED data at 20 K and by prior STM studies around 90 K.[5−7] A model consistent with this behavior is proposed. Upon adsorption, or during subsequent heating, clustering of molecular HCl is rapid, leading to the formation of 2D or 3D islands. The adsorbate is partially ordered with respect to the Pt(111) substrate, primarily due to the strength of the Pt−Cl interaction. By 100 K, molecular HCl has desorbed and the remaining HCl is dissociated. Dissociated chlorine (or chloride) is expected to have a much higher diffusion barrier than molecular HCl, and in large part, the islands retain the local clustering resulting from molecular interactions. HCl appears to dissociate below 100 K, but the data are insufficient to determine the kinetics of the process. We assign desorption for coverages of $\Theta > 0.25$ ML to be molecular, based on the width of the γ peak, the apparent first-order line shape, and the onset of H−Cl stretch for $\Theta = 0.28$ ML. Desorption for the γ peak is attributed to molecular HCl adjacent to the Pt(111) surface. At higher coverage, $\Theta > 0.38$ ML, the remaining two peaks, δ and ϵ, are attributed to desorption from molecular HCl adsorbed in the second layer, adjacent to the mixed dissociated and molecular HCl layer on the Pt(111) surface.

These results clearly show that for a monolayer of HCl on Pt(111) there are a number of coverage dependent adsorption states including both disociative and molecular. While a direct comparison of these data to electrochemical results is difficult because of solvent effects on the energetics, it is interesting to point out the work of Lipkowski et al. who observe a rich Gibbs excess energy dependence on potential (related to coverage) for HCl on Pt(111).[2] The complex adsorption behavior of HCl on platinum electrodes may be an important consideration for the design of electrochemical fuel cells.

Acknowledgment. We wish to acknowledge Zdenek Dohnálek for helpful scientific discussions. This work was supported by the U.S. Department of Energy, Basic Energy Sciences, Chemical Sciences Division. This work was performed at the W.R. Wiley Environmental Molecular Sciences Laboratory, a national scientific user facility sponsored by the Department of Energy's Office of Biological and Environmental Research and located at Pacific Northwest National Laboratory. Pacific Northwest National Laboratory is operated for the U.S. Department of Energy by Battelle under Contract No. DE-AC06-76RLO 1830. P.A. acknowledges support from FQRNT and CRSNG.

References and Notes

(1) Markovic, N. M.; Ross, P. N. *Surf. Sci. Rep.* **2002**, *45*, 121.
(2) Li, N. H.; Lipkowski, J. *J. Electroanal. Chem.* **2000**, *491*, 95.
(3) Lucas, C. A.; Markovic, N. M.; Ross, P. N. *Phy. Rev. B* **1997**, *55*, 7964.
(4) Wagner, F. T.; Moylan, T. E. *Surf. Sci.* **1989**, *216*, 361.
(5) Fukushima, T.; Song, M. B.; Ito, M. *Surf. Sci.* **2000**, *464*, 193.
(6) Nakamura, M.; Song, M. B.; Ito, M. *Chem. Phys. Lett.* **2000**, *320*, 381.
(7) Song, M. B.; Ito, M. *Bull. Korean Chem. Soc.* **2001**, *22*, 267.
(8) Ito, M.; Nakamura, M. *Faraday Discuss.* **2002**, *121*, 71.
(9) Nakamura, M.; Shingaya, Y.; Ito, M. *Surf. Sci.* **2002**, *502*, 474.
(10) Schennach, R.; Bechtold, E. *Surf. Sci.* **1997**, *380*, 9.
(11) Erley, W. *Surf. Sci.* **1980**, *94*, 281.
(12) Garwood, G. A.; Hubbard, A. T. *Surf. Sci.* **1981**, *112*, 281.
(13) Honig, R. E.; Hook, H. O. *RCA Rev.* **1960**, *21*, 360.
(14) Kay, B. D.; Lykke, K. R.; Creighton, J. R.; Ward, S. J. *J. Chem. Phys.* **1989**, *91*, 5120.
(15) Stampfl, C.; Kreuzer, H. J.; Payne, S. H.; Pfnur, H.; Scheffler, M. *Phys. Rev. Lett.* **1999**, *83*, 2993.
(16) Maschhoff, B. L.; Ledema, M. J.; Kwini, M.; Cowin, J. P. *Surf. Sci.* **1996**, *359*, 253.
(17) Livneh, T.; Asscher, M. *Langmuir* **1998**, *14*, 1348.
(18) Schlichting, H.; Menzel, D. *Rev. Sci. Instrum.* **1993**, *64*, 2013.
(19) Daschbach, J. L.; Peden, B. M.; Smith, R. S.; Kay, B. D. *J. Chem. Phys.* **2004**, *120*, 1516.
(20) King, D. A.; Wells, M. G. *Surf. Sci.* **1972**, *29*, 454.
(21) Polanyi, M.; Wigner, E. *Z. Phys. Chem.* **1928**, *139*, 439.
(22) Dohnalek, Z.; Kimmel, G. A.; Joyce, S. A.; Ayotte, P.; Smith, R. S.; Kay, B. D. *J. Phys. Chem. B* **2001**, *105*, 3747.
(23) Hornig, D. F.; Oserg, W. E. *J. Chem. Phys.* **1955**, *23*, 662.
(24) Hunka, D. E.; Herman, D. C.; Lopez, L. I.; Lormand, K. D.; Land, D. P. *J. Phys. Chem. B* **2001**, *105*, 4973.
(25) Bishop, D. M.; Norman, P. *J. Chem. Phys.* **1999**, *111*, 3042.
(26) *CRC Handbook of Chemistry and Physics*, 60th ed.; Weast, R. C., Ed.; CRC Press: Boca Raton, FL, 1979.
(27) Henderson, M. A.; Mitchell, G. E.; White, J. M. *Surf. Sci.* **1987**, *184*, L325.
(28) Kimmel, G. A.; Persson, M.; Dohnalek, Z.; Kay, B. D. *J. Chem. Phys.* **2003**, *119*, 6776.